Pergamon

Int. J. Solids Structures Vol. 33, No. 18, pp. 2625–2645, 1996

0020–7683/96 $15.00 + .00

0020-7683(95)00175-1

TRANSONIC CRACK GROWTH ALONG A BIMATERIAL INTERFACE: AN INVESTIGATION OF THE ASYMPTOTIC STRUCTURE OF NEAR-TIP FIELDS

Y. HUANG
Department of Mechanical Engineering and Engineering Mechanics, Michigan Technological University, Houghton, MI 49931, U.S.A.

C. LIU
Los Alamos National Laboratory, Los Alamos, NM 87545, U.S.A.

and

A. J. ROSAKIS
Graduate Aeronautical Laboratories, California Institute of Technology, Pasadena, CA 91125, U.S.A.

(*Received* 30 *November* 1994; *in revised form* 6 *June* 1995)

Abstract—Transonic interfacial crack growth in bimaterial systems is analysed, and the asymptotic field around the moving crack tip is obtained by the straightforward approach of analytic continuation. The power of singularity is less than 1/2 for anti-plane shear deformation. For in-plane deformation, the power of singularity can be real or complex, depending on the speed of the crack tip. Across the Rayleigh wave speed, the real part of the power has a jump of $-1/2$, and the imaginary part approaches infinity. The stresses are singular, not only around the crack tip, but also on an entire ray moving with the crack tip. These observations are illustrated by examples using PMMA/steel and Al/Al_2O_3 bimaterial systems. Copyright © 1996 Published by Elsevier Science Ltd.

1. INTRODUCTION

Numerous studies have been made of the dynamic interfacial fracture in the sub-Rayleigh speed regime, i.e. crack-tip speed lower than the Rayleigh wave speeds of each constituent in the bimaterial system [for example Gol'dstein (1967), Willis (1971, 1973), Brock and Achenbach (1973), Atkinson (1977), Yang *et al.* (1991), Wu (1991), Deng (1992) and Liu *et al.* (1993)]. It has been argued that the lower Rayleigh wave speed of the two constituents should be the terminal speed for interfacial crack propagation. Yang *et al.* (1991) convincingly showed, using an energy consideration, that dynamic debonding beyond the lower Rayleigh wave speed is admissible. The experimental studies on PMMA/steel bimaterial systems by Liu *et al.* (1993) and Lambros and Rosakis (1995) demonstrate that the crack-tip speed can be greater than, not only the lower Rayleigh wave speed, but also the lower shear wave speed.

Motivated by these experimental observations for PMMA/steel bimaterial systems, Liu *et al.* (1995) studied the asymptotic field near the transonically moving interfacial crack tip for an elastic solid bonded to a rigid substrate. This simplification of representing a stiffer constituent in the bimaterial system as a rigid substrate originated from the high elastic mismatch for the PMMA/steel system, $\mu^{\text{steel}}/\mu^{\text{PMMA}} = 66.7$, where μ is the shear modulus.

Very recently, it has come to our attention that Yu and Yang (1994) have obtained the near-tip asymptotic field for an out-of-plane shear (mode III) propagating crack running at a speed between the shear speeds of the constituents of the bimaterial interface. This study, which follows an entirely different methodology than the one presented in Section 2 of the current work, was conducted in parallel to our own investigation.

Since our work was motivated purely by experiments performed at Caltech over the past 5 years, our analytical emphasis is mainly directed toward investigating features of the near-crack-tip field that are easily identifiable by experimental measurements. As will become apparent, our work seeks to identify crack growth regimes where phenomena such as large-scale contact or the existence of lines of singularity emanating from the crack tip exist. These are features that seem to depend on crack-tip speed and were first observed in the experiments of Lambros and Rosakis (1995). In addition, the aim of the present study also includes the mathematical investigation of asymptotic fields surrounding a transonically moving interfacial crack tip for a general bimaterial system. In order to illustrate the properties of the near-tip fields, we choose to present results for the powers of singularity and oscillation and the angular stress distributions for bimaterials of some practical significance. These include a PMMA/steel system, which allows direct comparison with the dynamic experiments (Lambros and Rosakis, 1995), and an Al/Al_2O_3 system, which is a classical system often used in quasistatic investigations.

For the in-plane cases, the velocity regime studied is limited to the range $c_s^{(1)} < v < \min[c_s^{(2)}, c_\ell^{(1)}]$. Our choice is again motivated by experimentation, which does not show any evidence of transonic crack growth with velocities outside this range.

2. ANTI-PLANE SHEAR DEFORMATION

In the absence of body force density, the elastodynamic displacement field in a fixed orthogonal Cartesian coordinate system, $u_i(x_1, x_2, x_3, t)$ $(i = 1, 2, 3)$, is called anti-plane shear if the components of the displacement field are such that

$$\begin{aligned} u_\alpha(x_1, x_2, x_3, t) &= 0, \quad \alpha = 1, 2 \\ u_3(x_1, x_2, x_3, t) &= w(x_1, x_2, t). \end{aligned} \tag{1}$$

For the anti-plane shear deformation, the non-zero components of strain and stress are related to the function $w(x_1, x_2, t)$ by

$$\begin{aligned} \varepsilon_{3\alpha}(x_1, x_2, t) &= \tfrac{1}{2} w_{,\alpha}(x_1, x_2, t) \\ \sigma_{3\alpha}(x_1, x_2, t) &= \mu w_{,\alpha}(x_1, x_2, t), \quad \alpha = 1, 2 \end{aligned} \tag{2}$$

where μ is the shear modulus of the elastic solid. The equation of motion becomes

$$w_{,\alpha\alpha}(x_1, x_2, t) = \frac{1}{c_s^2} \ddot{w}(x_1, x_2, t) \tag{3}$$

where c_s is the shear wave speed of the solid and $c_s = \sqrt{\mu/\rho}$ (ρ is the mass density).

Consider a bimaterial system composed of two homogeneous, isotropic, and linearly elastic solids. Also, these two different materials are bonded along a straight interface and undergo anti-plane shear deformation. Without a loss of generality, it is assumed that $c_s^{(1)} < c_s^{(2)}$, where the superscripts 1 and 2 indicate the materials above or below the interface, respectively (Fig. 1). An interfacial crack propagates along the interface with speed v, such that

$$c_s^{(1)} < v < c_s^{(2)}. \tag{4}$$

As a result, the interfacial crack growth is transonic.

Both $w^{(1)}(x_1, x_2, t)$ and $w^{(2)}(x_1, x_2, t)$ satisfy the equation of motion (3) in the corresponding half-planes. By introducing the moving coordinate system $(\eta_1, \eta_2) = (x_1 - vt, x_2)$ and assuming that the crack growth is steady state, the equation of motion becomes

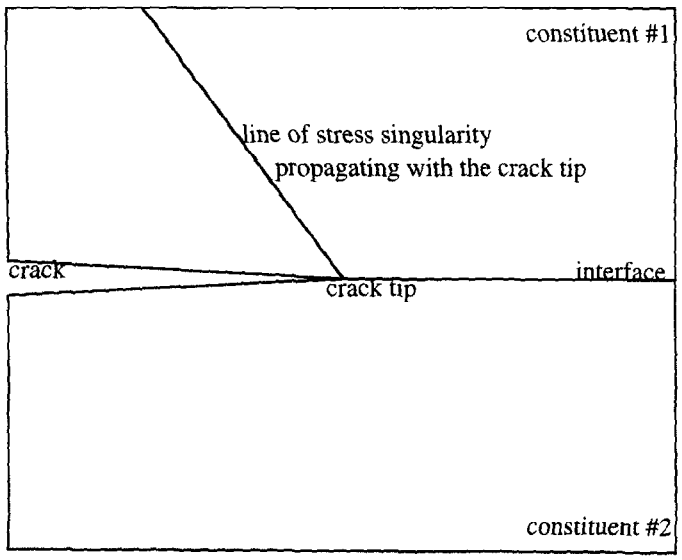

Fig. 1. Transonic crack growth along a bimaterial interface; shear wave speeds $c_s^{(1)} < c_s^{(2)}$ for bimaterial systems.

$$w^{(1)}_{,11}(\eta_1,\eta_2) - \frac{1}{\hat{\alpha}_{s1}^2} w^{(1)}_{,22}(\eta_1,\eta_2) = 0 \tag{5}$$

$$w^{(2)}_{,11}(\eta_1,\eta_2) + \frac{1}{\alpha_{s2}^2} w^{(2)}_{,22}(\eta_1,\eta_2) = 0 \tag{6}$$

where

$$\hat{\alpha}_{s1} = \left[\left(\frac{v}{c_s^{(1)}}\right)^2 - 1\right]^{1/2}, \quad \alpha_{s2} = \left[1 - \left(\frac{v}{c_s^{(2)}}\right)^2\right]^{1/2}. \tag{7}$$

It is clear that eqn (5) is hyperbolic and that eqn (6) is elliptical.

The most general solution to eqn (5) can be expressed as

$$w^{(1)}(\eta_1,\eta_2) = g(\eta_1 + \hat{\alpha}_{s1}\eta_2) + \overset{*}{g}(\eta_1 - \hat{\alpha}_{s1}\eta_2) \tag{8}$$

where $g(\eta_1 + \hat{\alpha}_{s1}\eta_2)$ and $\overset{*}{g}(\eta_1 - \hat{\alpha}_{s1}\eta_2)$ are real functions of their respective arguments. Similar to supersonic flow in aerodynamics, a material point ahead of the crack tip does not feel the disturbance from the transonically moving crack, and one finds

$$\overset{*}{g}(\eta_1 - \hat{\alpha}_{s1}\eta_2) = 0.$$

Hence,

$$w^{(1)}(\eta_1,\eta_2) = g(\eta_1 + \hat{\alpha}_{s1}\eta_2). \tag{9}$$

On the other hand, the most general solution to eqn (6) can be expressed as

$$w^{(2)}(\eta_1,\eta_2) = \mathrm{Re}\,[F(z_{s2})] \tag{10}$$

where $z_{s2} = \eta_1 + i\alpha_{s2}\eta_2$, Re stands for the real part of the argument, and $F(z_{s2})$ is an analytic function in the lower z_{s2} plane, i.e. $\alpha_{s2}\eta_2 \leqslant 0$.

Now in terms of the functions $g(\eta_1+\hat{\alpha}_{s1}\eta_2)$ and $F(z_{s2})$, the continuity of the displacement and traction across the interface can be written as

$$2g(\eta_1)-[F^-(\eta_1)+\bar{F}^+(\eta_1)]=0, \quad \text{for } \eta_1>0 \tag{11a}$$

$$2\hat{\alpha}_{s1}\mu^{(1)}g'(\eta_1)-i\alpha_{s2}\mu^{(2)}[F'^-(\eta_1)-\bar{F}'^+(\eta_1)]=0, \quad \text{for } \eta_1>0 \tag{11b}$$

where the overbar denotes a complex conjugate and the following notation has been used:

$$\Omega^{\pm}(\eta_1)=\lim_{\eta_2\to 0^{\pm}}\Omega(z), \quad z=\eta_1+i\eta_2.$$

Eliminating the function $g(\eta_1)$, one gets

$$(1-i\beta)\bar{F}'^+(\eta_1)-(1+i\beta)F'^-(\eta_1)=0, \quad \text{for } \eta_1>0 \tag{12}$$

where $\beta=\hat{\alpha}_{s1}\mu^{(1)}/\alpha_{s2}\mu^{(2)}$. By analytic continuation, eqn (12) leads to a new function, $\theta(z)$, which is analytic in the entire plane, except on the crack surface,

$$\theta(z)=\begin{cases}(1-i\beta)\bar{F}'(z), & \mathrm{Im}(z)>0\\ (1+i\beta)F'(z), & \mathrm{Im}(z)<0.\end{cases} \tag{13}$$

The traction-free boundary conditions on the crack surface take the form

$$g'(\eta_1)=0, \quad \text{for } \eta_1<0 \tag{14a}$$

$$F'^-(\eta_1)-\bar{F}'^+(\eta_1)=0, \quad \text{for } \eta_1<0. \tag{14b}$$

Using the new function, $\theta(z)$, eqn (14b) becomes

$$\theta^+(\eta_1)-\frac{1-i\beta}{1+i\beta}\theta^-(\eta_1)=0, \quad \text{for } \eta_1<0 \tag{15}$$

which represents a Riemann–Hilbert equation. The solution to this equation, which also complies with the requirement of bounded displacement, or $|\theta(z)|=O(|z|^{\alpha})$, as $|z|\to 0$ for some $\alpha>-1$, is

$$\theta(z)=\frac{A(z)}{z^{q(v)}}, \quad q(v)=\frac{1}{\pi}\tan^{-1}\frac{\hat{\alpha}_{s1}\mu^{(1)}}{\alpha_{s2}\mu^{(2)}} \tag{16}$$

where $A(z)$ is an arbitrary entire function. The power q is the order of singularity for stresses around the crack tip subjected to anti-plane shear deformation, and it increases monotonically from $q=0$ to $q=1/2$ as the crack propagating speed, v, increases from $c_s^{(1)}$ to $c_s^{(2)}$. From eqn (13), one has

$$\bar{F}'(z)=\frac{1}{1-i\beta}\cdot\frac{A(z)}{z^{q(v)}}, \quad \mathrm{Im}(z)>0 \tag{17a}$$

$$F'(z)=\frac{1}{1+i\beta}\cdot\frac{A(z)}{z^{q(v)}}, \quad \mathrm{Im}(z)<0. \tag{17b}$$

Thus, $A(z)=\bar{A}(z)$.

Returning to eqn (11a), one finds

$$g'(\eta_1) = \frac{1}{1+\beta^2} \cdot \frac{A(\eta_1)}{\eta_1^{q(v)}}, \quad \text{for } \eta_1 > 0 \tag{18}$$

and, together with eqn (14a), one has

$$g'(\eta_1) = \frac{1}{1+\beta^2} \cdot \frac{A(\eta_1)}{\eta_1^{q(v)}} H(\eta_1) \tag{19}$$

where $H(\cdot)$ is the Heaviside step function. If one is only concerned with the leading term in the steady-state solution and rigid-body motion is neglected, one can get the expressions for $w^{(1)}(\eta_1, \eta_2)$ and $w^{(2)}(\eta_1, \eta_2)$:

$$w^{(1)}(\eta_1, \eta_2) = \frac{1}{1+\beta^2} \cdot \frac{A_0}{1-q(v)} (\eta_1 + \hat{\alpha}_{s1}\eta_2)^{1-q(v)} H(\eta_1 + \hat{\alpha}_{s1}\eta_2) \tag{20a}$$

$$w^{(2)}(\eta_1, \eta_2) = \frac{1}{1+\beta^2} \cdot \frac{A_0}{1-q(v)} r_{s2}^{1-q(v)} \{\cos[1-q(v)]\theta_{s2} + \beta \sin[1-q(v)]\theta_{s2}\} \tag{20b}$$

where the scaled polar coordinate system (r_{s2}, θ_{s2}) is defined by $z_{s2} = r_{s2} e^{i\theta}_{s2}$ and is related to Cartesian coordinate (η_1, n_2) by

$$r_{s2} = (\eta_1^2 + \alpha_{s2}^2 \eta_2^2)^{1/2}, \quad \theta_{s2} = \tan^{-1} \frac{\alpha_{s2}\eta_2}{\eta_1} \tag{21}$$

and A_0 is an arbitrary real number.

For the limit $\mu^{(1)}/\mu^{(2)} = 1$ and $\rho^{(1)}/\rho^{(2)} = 1$, the bimaterial system degenerates to a homogeneous solid. For the other limit, $\mu^{(1)}/\mu^{(2)} = 0$, the substrate becomes a rigid solid. It is interesting to observe that these two limiting cases have the same equation of motion, eqn (5), and exactly the same boundary conditions:

$$\left.\frac{\partial w}{\partial \eta_2}\right|_{\substack{\eta_2 \to 0^+ \\ \eta_1 < 0}} = 0 \tag{22a}$$

$$\left. w \right|_{\substack{\eta_2 \to 0^+ \\ \eta_1 > 0}} = 0. \tag{22b}$$

The only displacement field in eqn (9) satisfying these boundary conditions is $w = 0$ since the entire system is hyperbolic. This means a crack cannot propagate transonically in homogeneous or elastic/rigid solids under anti-plane shear conditions.

The stresses are singular at the crack tip, as expected. Moreover, from eqn (20a) for the upper half-plane, the left wedge ($\eta_1 + \hat{\alpha}_{s1}\eta_2 < 0$) is stress free, while the stresses to the right of the wedge are singular on the entire ray $\eta_1 + \hat{\alpha}_{s1}\eta_2 = 0$ instead of on a single point—the crack tip. This distinct feature of a line of singularity propagating with the crack tip is unique for transonic crack growth.

The power of singularity, q, as given in eqn (16) is shown vs the normalized crack speed, $v/c_s^{(1)}$, in Fig. 2 for two bimaterial systems, PMMA/steel and Al/Al_2O_3. Crack growth in the PMMA/steel system was studied by Liu *et al.* (1993) and by Lambros and Rosakis (1995), and Al/Al_2O_3 is an example of a ceramic matrix composite (Evans and Marshall, 1989). The mechanical properties and shear wave speeds for these materials are given in Table 1. The crack speed, v, can vary between the two shear wave speeds for the bimaterial. For the PMMA/steel system, the singularity is rather weak for a wide range of crack speeds due to large elastic mismatch, and the singularity increases sharply as v approaches the shear wave speed of steel.

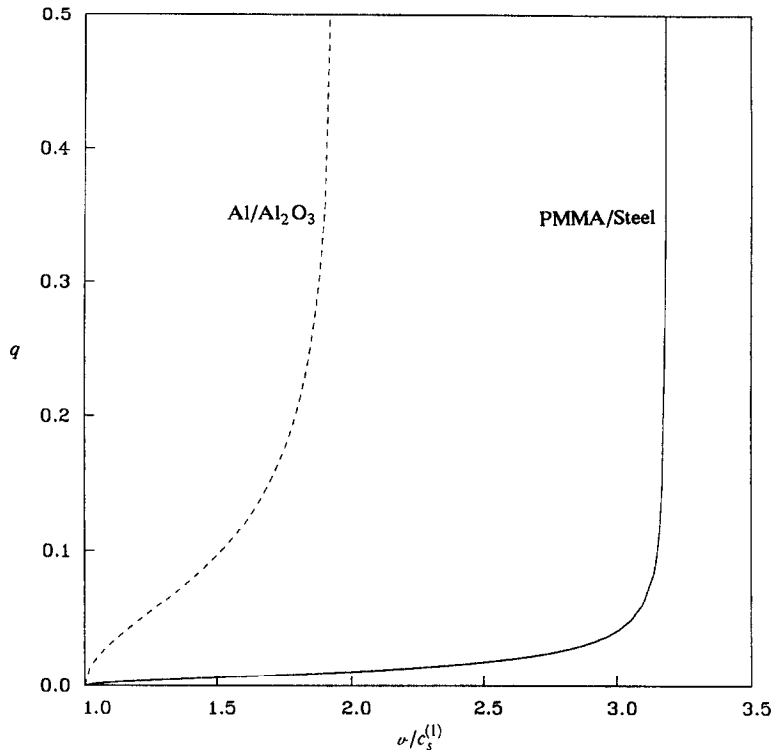

Fig. 2. Power of singularity, q, vs the normalized interfacial crack speed, $v/c_s^{(1)}$, for PMMA/steel (solid line) and Al/Al_2O_3 (dashed line) bimaterial systems with anti-plane deformation; crack speed in the range $[c_s^{PMMA}, c_s^{steel}]$ and $[c_s^{Al}, c_s^{Al_2O_3}]$, respectively.

Table 1. Properties and wave speeds of selected materials

	Shear modulus μ (GPa)	Poisson's ratio ν	Density ρ (kg m^{-3})	Shear wave speeds c_s (m s^{-1})	Longitudinal wave speeds	
					Plane stress c_ℓ (m s^{-1})	Plane strain c_ℓ (m s^{-1})
PMMA	1.2	0.35	1190	1004	1761	2090
AISI 4340 Steel	80.0	0.30	7833	3196	5402	5979
Al	26.3	0.33	2700	3122	5394	6198
Al_2O_3	151.0	0.26	4200	5992	9851	10521

It is noted that the scaled polar coordinate (r_{s2}, θ_{s2}) in eqn (21) can be written in terms of polar coordinates (r, θ) as

$$r_{s2} = r(\cos^2\theta + \alpha_{s2}^2 \sin^2\theta)^{1/2}, \quad \theta_{s2} = \tan^{-1}(\alpha_{s2}\tan\theta).$$

Hence, the dependence of the shear stresses on polar radius r and polar angle θ are separated, i.e.

$$\sigma_{3\alpha} = \frac{\mu}{1+\beta^2}\frac{A_0}{r^{q(v)}}\tilde{\gamma}_\alpha(\theta) \quad \alpha = 1, 2 \tag{23}$$

where the non-dimensional functions $\tilde{\gamma}_\alpha$ satisfy $\tilde{\gamma}_1(\theta = 0) = 1$. Functions $\tilde{\gamma}_\alpha(\theta)$ $(\alpha = 1, 2)$ represent the angular distributions of shear strains and depend on the polar angle θ in addition to crack speed and bimaterial properties. The remote loading distributions only influence the near-tip stress field through the constant A_0. Functions $\tilde{\gamma}_1(\theta)$ and $\tilde{\gamma}_2(\theta)$ are

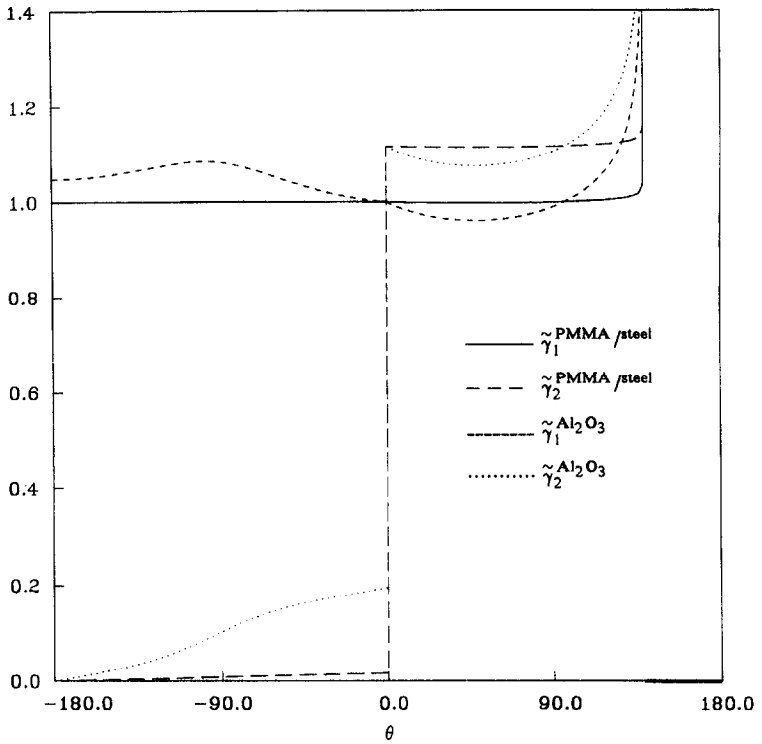

Fig. 3. The angular distribution of normalized strains, γ_α ($\alpha = 1, 2$), for PMMA/steel (solid line = $\tilde{\gamma}_1$; long dashed line = $\tilde{\gamma}_2$) and Al/Al_2O_3 (dashed line = $\tilde{\gamma}_1$; dotted line = $\tilde{\gamma}_2$) bimaterial systems with anti-plane deformation, $v = 1.5c_s^{(1)}$.

shown vs all ranges of the polar angle ($-180° < \theta < 180°$) in Fig. 3 for PMMA/steel and Al/Al_2O_3 systems for $v/c_s^{(1)} = 1.5$. A discontinuity of $\tilde{\gamma}_2(\theta)$ exists across the interface ($\theta = 0$) because of the elastic mismatch. It is clearly seen that the variations of $\tilde{\gamma}_\alpha$ are relatively small (except for the jump) until the wedge boundary, $\theta = 90° + \tan^{-1}\hat{\alpha}_{s1}$, is approached.

3. IN-PLANE DEFORMATION

The in-plane elastodynamic field is considered in this section. The displacements are independent of x_3 in any fixed coordinate system (x_1, x_2). The in-plane displacements can be expressed using two displacement potentials, ϕ and ψ, as

$$u_1(x_1, x_2, t) = \frac{\partial \phi(x_1, x_2, t)}{\partial x_1} + \frac{\partial \psi(x_1, x_2, t)}{\partial x_2} \tag{24a}$$

$$u_2(x_1, x_2, t) = \frac{\partial \phi(x_1, x_2, t)}{\partial x_2} - \frac{\partial \psi(x_1, x_2, t)}{\partial x_1}. \tag{24b}$$

The strains and stresses can be given as

$$\varepsilon_{11} = \phi_{,11} + \psi_{,12}, \quad \varepsilon_{22} = \phi_{,22} - \psi_{,12}, \quad \varepsilon_{12} = \phi_{,12} + \tfrac{1}{2}(\psi_{,22} - \psi_{,11}) \tag{25a}$$

$$\sigma_{11} = \mu\left(\frac{\kappa+1}{\kappa-1}\varepsilon_{11} + \frac{3-\kappa}{\kappa-1}\varepsilon_{22}\right), \quad \sigma_{22} = \mu\left(\frac{\kappa+1}{\kappa-1}\varepsilon_{22} + \frac{3-\kappa}{\kappa-1}\varepsilon_{11}\right), \quad \sigma_{12} = 2\mu\varepsilon_{12} \tag{25b}$$

where μ is the shear modulus, $\kappa = 3 - 4\nu$ for plane strain, $\kappa = (3-\nu)/(1+\nu)$ for plane stress, and ν is the Poisson's ratio. The equation of motion becomes

$$\phi_{,\alpha\alpha}(x_1, x_2, t) = \ddot{\phi}(x_1, x_2, t) \tag{26}$$

and

$$\psi_{,\alpha\alpha}(x_1, x_2, t) = \ddot{\psi}(x_1, x_2, t). \tag{27}$$

Besides the shear wave speed, $c_s = \sqrt{\mu/\rho}$, there is another speed in the in-plane deformation—the longitudinal wave speed, $c_\ell = [(\kappa+1)/(\kappa-1)]^{1/2} c_s$.

Consider the bimaterial system in Fig. 1. Without a loss of generality, it is assumed that $c_s^{(1)} < c_s^{(2)}$, where the superscripts 1 and 2 indicate materials above and below the interface, respectively. An interfacial crack propagates transonically with speed v such that

$$c_s^{(1)} < v < \min [c_s^{(2)}, \ c_\ell^{(1)}] \tag{28}$$

where min stands for the minimum of $c_s^{(2)}$ and $c_\ell^{(1)}$. By introducing the moving coordinate $(\eta_1, \eta_2) = (x_1 - vt, \ x_2)$ and assuming that crack growth is steady-state, the equations of motion become

$$\phi^{(1)}_{,11}(\eta_1, \eta_2) + \frac{1}{\alpha_{\ell 1}^2} \phi^{(1)}_{,22}(\eta_1, \eta_2) = 0 \quad \text{for } \eta_2 > 0 \tag{29}$$

$$\psi^{(1)}_{,11}(\eta_1, \eta_2) - \frac{1}{\hat{\alpha}_{s1}^2} \psi^{(1)}_{,22}(\eta_1, \eta_2) = 0 \quad \text{for } \eta_2 > 0 \tag{30}$$

and

$$\phi^{(2)}_{,11}(\eta_1, \eta_2) + \frac{1}{\alpha_{\ell 2}^2} \phi^{(2)}_{,22}(\eta_1, \eta_2) = 0 \quad \text{for } \eta_2 < 0 \tag{31}$$

$$\psi^{(2)}_{,11}(\eta_1, \eta_2) + \frac{1}{\alpha_{s2}^2} \psi^{(2)}_{,22}(\eta_1, \eta_2) = 0 \quad \text{for } \eta_2 < 0 \tag{32}$$

where $\hat{\alpha}_{s1}$ and α_{s2} are the same as in eqn (7) and $\alpha_{\ell 1}$ and $\alpha_{\ell 2}$ are given as

$$\alpha_{\ell 1} = \left[1 - \left(\frac{v}{c_\ell^{(1)}}\right)^2\right]^{1/2}, \quad \alpha_{\ell 2} = \left[1 - \left(\frac{v}{c_\ell^{(2)}}\right)^2\right]^{1/2}. \tag{33}$$

It is clear that eqn (30) is hyperbolic and that eqns (29), (31), and (32) are elliptical. Similar to the discussion in the previous section, the general solutions to these equations are

$$\phi^{(1)}(\eta_1, \eta_2) = \text{Re}\,[F_1(z_{\ell 1})] \tag{34}$$

$$\psi^{(1)}(\eta_1, \eta_2) = g(\eta_1 + \hat{\alpha}_{s1}\eta_2) \tag{35}$$

$$\phi^{(2)}(\eta_1, \eta_2) = \text{Re}\,[F_2(z_{\ell 2})] \tag{36}$$

$$\psi^{(2)}(\eta_1, \eta_2) = \text{Im}\,[G_2(z_{s2})] \tag{37}$$

where $z_{\ell 1} = \eta_1 + i\alpha_{\ell 1}\eta_2$; $z_{\ell 2} = \eta_1 + i\alpha_{\ell 2}\eta_2$; $z_{s2} = \eta_1 + i\alpha_{s2}\eta_2$; Re and Im stand for the real and imaginary parts of the argument, respectively; $F_1(z_{\ell 1})$ is an analytic function in the upper $z_{\ell 1}$ plane ($\alpha_{\ell 1}\eta_2 \geqslant 0$); and $F_2(z_{\ell 2})$ and $G_2(z_{s2})$ are analytic functions of $z_{\ell 2}$ and z_{s2} in the corresponding lower half-plane ($\alpha_{\ell 2}\eta_2 \leqslant 0$, $\alpha_{s2}\eta_2 \leqslant 0$), respectively.

The displacements can be derived from eqn (24),

$$u_1^{(1)} = \mathrm{Re}\,[F_1'(z_{\ell 1})] + \hat{\alpha}_{s1} g'(\eta_1 + \hat{\alpha}_{s1}\eta_2) \tag{38a}$$

$$u_2^{(1)} = -\alpha_{\ell 1}\,\mathrm{Im}\,[F_1'(z_{\ell 1})] - g'(\eta_1 + \hat{\alpha}_{s1}\eta_2) \tag{38b}$$

and

$$u_1^{(2)} = \mathrm{Re}\,[F_2'(z_{\ell 2}) + \hat{\alpha}_{s2} G_2'(z_{s2})] \tag{39a}$$

$$u_2^{(2)} = -\mathrm{Im}\,[\alpha_{\ell 2} F_2'(z_{\ell 2}) + G_2'(z_{s2})]. \tag{39b}$$

The stresses are given by eqn (25b) as

$$\sigma_{11}^{(1)} = \mu^{(1)}\{(1 + 2\alpha_{\ell 1}^2 + \hat{\alpha}_{s1}^2)\,\mathrm{Re}\,[F_1''(z_{\ell 1})] + 2\hat{\alpha}_{s1} g''(\eta_1 + \hat{\alpha}_{s1}\eta_2)\} \tag{40a}$$

$$\sigma_{22}^{(1)} = -\mu^{(1)}\{(1 - \hat{\alpha}_{s1}^2)\,\mathrm{Re}\,[F_1''(z_{\ell 1})] + 2\hat{\alpha}_{s1} g''(\eta_1 + \hat{\alpha}_{s1}\eta_2)\} \tag{40b}$$

$$\sigma_{12}^{(1)} = -\mu^{(1)}\{2\alpha_{\ell 1}\,\mathrm{Im}\,[F_1''(z_{\ell 1})] + (1 - \hat{\alpha}_{s1}^2) g''(\eta_1 + \hat{\alpha}_{s1}\eta_2)\} \tag{40c}$$

and

$$\sigma_{11}^{(2)} = \mu^{(2)}\,\mathrm{Re}\,[(1 + 2\alpha_{\ell 2}^2 - \alpha_{s2}^2) F_2''(z_{\ell 2}) + 2\alpha_{s2} G_2''(z_{s2})] \tag{41a}$$

$$\sigma_{22}^{(2)} = -\mu^{(2)}\,\mathrm{Re}\,[(1 + \alpha_{s2}^2) F_2''(z_{\ell 2}) + 2\alpha_{s2} G_2''(z_{s2})] \tag{41b}$$

$$\sigma_{12}^{(2)} = -\mu^{(2)}\,\mathrm{Im}\,[2\alpha_{\ell 2} F_2''(z_{\ell 2}) + (1 + \alpha_{s2}^2) G_2''(z_{s2})]. \tag{41c}$$

Now, from eqns (38) and (39), the continuity of displacements across the interface, $[[u_1]] = 0$ and $[[u_2]] = 0$, can be written as

$$F_1'^{+}(\eta_1) + \bar{F}_1'^{-}(\eta_1) + 2\hat{\alpha}_{s1} g'(\eta_1) = F_2'^{-}(\eta_1) + \bar{F}_2'^{+}(\eta_1) + \alpha_{s2}[G_2'^{-}(\eta_1) + \bar{G}_2'^{+}(\eta_1)] \quad \text{for } \eta_1 > 0 \tag{42a}$$

$$\alpha_{\ell 1}[F_1'^{+}(\eta_1) - \bar{F}_1'^{-}(\eta_1)] + 2ig'(\eta_1) = \alpha_{\ell 2}[F_2'^{-}(\eta_1) - \bar{F}_2'^{+}(\eta_1)] + G_2'^{-}(\eta_1) - \bar{G}_2'^{+}(\eta_1) \quad \text{for } \eta_1 > 0. \tag{42b}$$

From eqns (40) and (41), the continuity of stresses across the interface, $[[\sigma_{12}]] = 0$ and $[[\sigma_{22}]] = 0$, can be written as

$$2\gamma\alpha_{\ell 1}[F_1''^{+}(\eta_1) - \bar{F}_1''^{-}(\eta_1)] + 2i\gamma(1 - \hat{\alpha}_{s1}^2) g''(\eta_1) = 2\alpha_{\ell 2}[F_2''^{-}(\eta_1) - \bar{F}_2''^{+}(\eta_1)] + (1 + \alpha_{s2}^2)[G_2''^{-}(\eta_1) - \bar{G}_2''^{+}(\eta_1)] \quad \text{for } \eta_1 > 0 \tag{42c}$$

$$\gamma(1 - \hat{\alpha}_{s1}^2)[F_1''^{+}(\eta_1) + \bar{F}_1''^{-}(\eta_1)] + 4\gamma\hat{\alpha}_{s1} g''(\eta_1) = (1 + \alpha_{s2}^2)[F_2''^{-}(\eta_1) + \bar{F}_2''^{+}(\eta_1)] + 2\alpha_{s2}[G_2''^{-}(\eta_1) + \bar{G}_2''^{+}(\eta_1)] \quad \text{for } \eta_1 > 0 \tag{42d}$$

where $\gamma = \mu^{(1)}/\mu^{(2)}$.

Equation (42b) is used to eliminate $g(\eta_1)$ from eqns (42a,c,d), which can then be rearranged in the following matrix form:

$$\mathbf{M}\begin{pmatrix} F_1''^{+}(\eta_1) \\ \bar{F}_2''^{+}(\eta_1) \\ \bar{G}_2''^{+}(\eta_1) \end{pmatrix} - \bar{\mathbf{M}}\begin{pmatrix} \bar{F}_1''^{-}(\eta_1) \\ F_2''^{-}(\eta_1) \\ G_2''^{-}(\eta_1) \end{pmatrix} = \mathbf{0} \tag{43}$$

where

$$\mathbf{M}=\begin{pmatrix}\gamma[2\hat{\alpha}_{s1}\alpha_{\ell 1}-i(1-\hat{\alpha}_{s1}^2)] & 2\gamma\hat{\alpha}_{s1}\alpha_{\ell 2}+i(1+\alpha_{s2}^2) & 2\gamma\hat{\alpha}_{s1}+2i\alpha_{s2}\\ \gamma\alpha_{\ell 1}(1+\hat{\alpha}_{s1}^2) & \alpha_{\ell 2}[2-\gamma(1-\hat{\alpha}_{s1}^2)] & 1+\alpha_{s2}^2-\gamma(1-\hat{\alpha}_{s1}^2)\\ \hat{\alpha}_{s1}\alpha_{\ell 1}-i & \hat{\alpha}_{s1}\alpha_{\ell 2}+i & \hat{\alpha}_{s1}+i\alpha_{s2}\end{pmatrix}. \tag{44}$$

From analytical continuation, eqn (43) leads to a vector of three new functions, $\boldsymbol{\theta}(z)$, which is analytic in the entire plane except on the non-positive part of the real axis (i.e., the crack surface):

$$\boldsymbol{\theta}(z)=\mathbf{M}[F_1''(z),\bar{F}_2''(z),\bar{G}_2''(z)]^{\mathrm{T}}\quad\text{for Im}(z)>0 \tag{45a}$$

$$\boldsymbol{\theta}(z)=\bar{\mathbf{M}}[\bar{F}_1''(z),F_2''(z),G_2''(z)]^{\mathrm{T}}\quad\text{for Im}(z)<0 \tag{45b}$$

where the superscript T stands for the transposition. Equation (45) can also be written as

$$[F_1''(z),\bar{F}_2''(z),\bar{G}_2''(z)]^{\mathrm{T}}=\mathbf{M}^{-1}\boldsymbol{\theta}(z)\quad\text{for Im}(z)>0 \tag{46a}$$

$$[\bar{F}_1''(z),F_2''(z),G_2''(z)]^{\mathrm{T}}=\bar{\mathbf{M}}^{-1}\boldsymbol{\theta}(z)\quad\text{for Im}(z)<0. \tag{46b}$$

The traction-free condition on the upper crack surface ($\eta_1<0,\ \eta_2\to 0^+$) gives

$$\alpha_{\ell 1}[F_1''^{+}(\eta_1)-\bar{F}_1''^{-}(\eta_1)]+i(1-\hat{\alpha}_{s1}^2)g''(\eta_1)=0\quad\text{for }\eta_1<0 \tag{47a}$$

$$(1-\hat{\alpha}_{s1}^2)[F_1''^{+}(\eta_1)+\bar{F}_1''^{-}(\eta_1)]+4\hat{\alpha}_{s1}g''(\eta_1)=0\quad\text{for }\eta_1<0. \tag{47b}$$

Function g can be eliminated from eqn (47), giving

$$[4\hat{\alpha}_{s1}\alpha_{\ell 1}-i(1-\hat{\alpha}_{s1}^2)^2]F_1''^{+}(\eta_1)-[4\hat{\alpha}_{s1}\alpha_{\ell 1}+i(1-\hat{\alpha}_{s1}^2)^2]F_1''^{-}(\eta_1)=0\quad\text{for }\eta_1<0. \tag{48}$$

The traction-free condition on the lower crack surface ($\eta_1<0,\ \eta_2\to 0^-$) gives

$$2\alpha_{\ell 2}[F_2''^{-}(\eta_1)-\bar{F}_2''^{+}(\eta_1)]+(1+\alpha_{s2}^2)[G_2''^{-}(\eta_1)-\bar{G}_2''^{+}(\eta_1)]=0\quad\text{for }\eta_1<0 \tag{49a}$$

$$(1+\alpha_{s2}^2)[F_2''^{-}(\eta_1)+\bar{F}_2''^{+}(\eta_1)]+2\alpha_{s2}[G_2''^{-}(\eta_1)+\bar{G}_2''^{+}(\eta_1)]=0\quad\text{for }\eta_1<0. \tag{49b}$$

Equations (48) and (49) can be rearranged in the following matrix form:

$$\mathbf{P}\begin{pmatrix}F_1''^{+}(\eta_1)\\ \bar{F}_2''^{+}(\eta_1)\\ \bar{G}_2''^{+}(\eta_1)\end{pmatrix}-\bar{\mathbf{P}}\begin{pmatrix}\bar{F}_1''^{-}(\eta_1)\\ F_2''^{-}(\eta_1)\\ G_2''^{-}(\eta_1)\end{pmatrix}=0\quad\text{for }\eta_1<0 \tag{50}$$

where

$$\mathbf{P}=\begin{pmatrix}4\hat{\alpha}_{s1}\alpha_{\ell 1}-i(1-\hat{\alpha}_{s1}^2)^2 & 0 & 0\\ 0 & -i(1+\alpha_{s2}^2) & -2i\alpha_{s2}\\ 0 & 2\alpha_{\ell 2} & 1+\alpha_{s2}^2\end{pmatrix}. \tag{51}$$

Equation (50) can be rewritten in terms of the analytical function $\boldsymbol{\theta}(z)$ in eqn (46) as

$$\mathbf{P}\mathbf{M}^{-1}\boldsymbol{\theta}^{+}(\eta_1)-\bar{\mathbf{P}}\bar{\mathbf{M}}^{-1}\boldsymbol{\theta}^{-}(\eta_1)=0\quad\text{for }\eta_1<0 \tag{52}$$

where $\boldsymbol{\theta}^{\pm}(\eta_1)$ are the limits $\lim_{\eta_1<0,\eta_2\to 0^{\pm}}\theta(\eta_1+i\eta_2)$, respectively.

An auxiliary problem needs to be solved for eqn (52). Let λ_1, λ_2, and λ_3 be the eigenvalues and χ_1, χ_2, and χ_3 be the corresponding eigenvectors for the following eigenvalue problem:

$$\mathbf{P}\mathbf{M}^{-1}\chi - \lambda\bar{\mathbf{P}}\bar{\mathbf{M}}^{-1}\chi = 0. \tag{53}$$

The eigenvalues are determined by

$$\det\{\mathbf{P}\mathbf{M}^{-1} - \lambda\bar{\mathbf{P}}\bar{\mathbf{M}}^{-1}\} = 0 \tag{54}$$

which is a third-order algebraic equation for λ. The details of solutions for λ and the eigenvectors χ_1, χ_2, and χ_3 are provided in the Appendix. It is found that one eigenvalue, say λ_3, is identically one (1), and the other two, λ_1 and λ_2, are the solutions of the following quadratic equation:

$$A\lambda^2 + B\lambda + \bar{A} = 0 \tag{55}$$

where A and B are non-dimensional *complex* and *real* parameters, respectively, depending on bimaterial shear moduli ratio γ [$= \mu^{(1)}/\mu^{(2)}$] and on the crack speed v through the αs ($\hat{\alpha}_{s1}$, $\alpha_{\ell 1}$, α_{s2}, and $\alpha_{\ell 2}$) as given in the Appendix. The two eigenvalues are given by

$$\lambda_{1,2} = \frac{-B \pm \sqrt{B^2 - 4A\bar{A}}}{2A} \tag{56}$$

which satisfies $|\lambda_1||\lambda_2| = 1$. Moreover, since parameter B is real, eqn (55) can be rewritten as

$$A\left(\frac{1}{\bar{\lambda}}\right)^2 + B\frac{1}{\bar{\lambda}} + \bar{A} = 0.$$

Therefore, $1/\bar{\lambda}$ is also an eigenvalue. The conjugate of eigenequation (53) can also be rearranged as

$$\mathbf{P}\mathbf{M}^{-1}\bar{\chi} - \frac{1}{\bar{\lambda}}\bar{\mathbf{P}}\bar{\mathbf{M}}^{-1}\bar{\chi} = 0$$

which indicates that, if χ is the eigenvector for eigenvalue λ, $\bar{\chi}$ is the corresponding eigenvector for eigenvalue $1/\bar{\lambda}$. There are only two possibilities that need to be considered:

(i) $|\lambda_1| = 1$, hence $|\lambda_2| = 1$, $\lambda_1 = 1/\bar{\lambda}_1$, and $\lambda_2 = 1/\bar{\lambda}_2$, i.e. λ and $1/\bar{\lambda}$ are identical. From the discussion above, $\bar{\chi}_\alpha$ and χ_α are eigenvectors for the same eigenvalue λ_α ($\alpha = 1, 2$). The eigenvectors χ_1 and χ_2 can be taken as real.

(ii) $|\lambda_1| \neq 1$, hence $\lambda_1 = 1/\bar{\lambda}_2$, or $\lambda_2 = 1/\bar{\lambda}_1$. For the eigenvector χ_1 corresponding to λ_1, its conjugate $\bar{\chi}_1$ corresponds to $1/\bar{\lambda}_1 = \lambda_2$, i.e. the eigenvectors χ_1 and χ_2 are complex conjugates.

The eigenvector corresponding to the third eigenvalue, $\lambda_3 = 1$, can always be taken as real.

The analytic functions $\boldsymbol{\theta}(z)$ can be expanded in terms of the eigenvectors:

$$\boldsymbol{\theta}(z) = \theta_1(z)\chi_1 + \theta_2(z)\chi_2 + \theta_3(z)\chi_3 = (\chi_1, \chi_2, \chi_3)\begin{pmatrix}\theta_1(z)\\ \theta_2(z)\\ \theta_3(z)\end{pmatrix} \tag{57}$$

where the scalar functions $\theta_i(z)$ ($i = 1, 2, 3$) are analytic except on the crack surface. The

substitution of eqn (57) into the jump condition for $\boldsymbol{\theta}$, eqn (52), and the utilization of eqn (53) yield

$$\lambda_1\theta_1^+(\eta_1)-\theta_1^-(\eta_1)=0 \quad \text{for } \eta_1<0 \tag{58a}$$

$$\lambda_2\theta_2^+(\eta_1)-\theta_2^-(\eta_1)=0 \quad \text{for } \eta_1<0 \tag{58b}$$

$$\theta_3^+(\eta_1)-\theta_3^-(\eta_1)=0 \quad \text{for } \eta_1<0 \tag{58c}$$

where $\lambda_3=1$ has been used and $\lambda_{1,2}$ are given in eqn (56). This constitutes three Riemann–Hilbert problems. From the requirement of bounded displacement at the crack tip, or $|\theta(z)|=O(|z|^{\alpha})$ for some $\alpha>-1$, their solutions are

$$\theta_1(z)=\frac{A_1(z)}{z^{q_1}}, \quad \theta_2(z)=\frac{A_2(z)}{z^{q_2}}, \quad \theta_3(z)=A_3(z) \tag{59}$$

where $A_i(z)$ are entire functions, i.e. analytic in the entire plane, and

$$q_1=\frac{\ln\lambda_1}{2\pi\mathrm{i}}, \quad q_2=\frac{\ln\lambda_2}{2\pi\mathrm{i}} \tag{60}$$

where $\mathrm{Re}(q_1)<1$ and $\mathrm{Re}(q_2)<1$ from the requirement of bounded displacements at the crack tip. The third eigenvalue, $\lambda_3=1$, gives an entire function, $A_3(z)$, which leads to no singularity around the crack tip. Its asymptotic behavior corresponds to the T-stress parallel to the interface.

Functions F_1, F_2, and G_2 can be obtained by substituting eqns (57) and (59) into eqn (46):

$$[F_1''(z),\bar{F}_2''(z),\bar{G}_2''(z)]^{\mathrm{T}}=\mathbf{M}^{-1}(\boldsymbol{\chi}_1,\boldsymbol{\chi}_2,\boldsymbol{\chi}_3)\left[\frac{A_1(z)}{z^{q_1}},\frac{A_2(z)}{z^{q_2}},A_3(z)\right]^{\mathrm{T}} \quad \text{for } \mathrm{Im}(z)>0 \tag{61a}$$

$$[\bar{F}_1''(z),F_2''(z),G_2''(z)]^{\mathrm{T}}=\bar{\mathbf{M}}^{-1}(\boldsymbol{\chi}_1,\boldsymbol{\chi}_2,\boldsymbol{\chi}_3)\left[\frac{A_1(z)}{z^{q_1}},\frac{A_2(z)}{z^{q_2}},A_3(z)\right]^{\mathrm{T}} \quad \text{for } \mathrm{Im}(z)<0. \tag{61b}$$

Its comparison leads to

$$\frac{A_1(z)}{z^{q_1}}\boldsymbol{\chi}_1+\frac{A_2(z)}{z^{q_2}}\boldsymbol{\chi}_2+A_3(z)\boldsymbol{\chi}_3=\frac{\bar{A}_1(z)}{z^{\bar{q}_1}}\bar{\boldsymbol{\chi}}_1+\frac{\bar{A}_2(z)}{z^{\bar{q}_2}}\bar{\boldsymbol{\chi}}_2+\bar{A}_3(z)\bar{\boldsymbol{\chi}}_3. \tag{62}$$

For the first possibility of λ, $|\lambda_1|=1$ and $|\lambda_2|=1$, q_1 and q_2 are real, and all three eigenvectors are also real. Hence, from eqns (57) and (59), function $\boldsymbol{\theta}(z)$ involves real power such that there is no oscillation in displacement and stress fields near the crack tip. Equation (62) gives

$$A_1(z)=\bar{A}_1(z), \quad A_2(z)=\bar{A}_2(z), \quad A_3(z)=\bar{A}_3(z). \tag{63}$$

For $q_1>q_2$ and $q_1>0$, the most singular term is $1/z^{q_1}$, and the leading term in the asymptotic solution for $\boldsymbol{\theta}(z)$ is $A_{10}\boldsymbol{\chi}_1/z^{q_1}$, where A_{10} and $\boldsymbol{\chi}_1$ are real, and A_{10} represents the magnitude of the asymptotic field and depends on external loading and geometry. From eqn (46), one finds

$$\begin{pmatrix} F_1(z) \\ \bar{F}_2(z) \\ \bar{G}_2(z) \end{pmatrix} = \frac{A_{10}}{(1-q_1)(2-q_1)} z^{2-q_1} \mathbf{M}^{-1} \boldsymbol{\chi}_1. \tag{64}$$

In order to obtain displacement potentials $\phi^{(1)}$, $\phi^{(2)}$, and $\psi^{(2)}$, the argument z of functions F_1, F_2, and G_2 needs to be changed to $z_{\ell 1}$, $z_{\ell 2}$, and z_{s2}, respectively, as given in eqns (34), (36), and (37). The potential $\psi^{(1)} = g(\eta_1 + \hat{\alpha}_{s1}\eta_2)$ can be found in terms of F_1, F_2, and G_2 from eqn (42b) for $\eta_1 + \hat{\alpha}_{s1}\eta_2 > 0$ and in terms of F_1 from eqn (47b) for $\eta_1 + \hat{\alpha}_{s1}\eta_2 < 0$.

For the other possibility, $|\lambda_1| \neq 1$ and $\lambda_2 = 1/\bar{\lambda}_1$, q_1 and q_2 are complex conjugates and, consequently, there is oscillation in the near-tip fields. The eigenvectors have the relations $\boldsymbol{\chi}_1 = \bar{\boldsymbol{\chi}}_2$, $\boldsymbol{\chi}_3 = \bar{\boldsymbol{\chi}}_3$, hence eqn (62) gives

$$A_1(z) = \bar{A}_2(z), \quad A_3(z) = \bar{A}_3(z). \tag{65}$$

The leading term in the asymptotic solution for $\boldsymbol{\theta}(z)$ is $A'_{10}\boldsymbol{\chi}_1/z^{q_1} + \bar{A}'_{10}\bar{\boldsymbol{\chi}}_1/z^{\bar{q}_1}$ and the complex constant, A'_{10}, characterizes the magnitude of the asymptotic field. From eqn (46), one finds

$$\begin{pmatrix} F_1(z) \\ \bar{F}_2(z) \\ \bar{G}_2(z) \end{pmatrix} = \mathbf{M}^{-1}(A'_{10} z^{2-q_1}\boldsymbol{\chi}_1 + \bar{A}'_{10} z^{2-\bar{q}_1}\bar{\boldsymbol{\chi}}_1) \frac{1}{(1-q_1)(2-q_1)}. \tag{66}$$

The conditions governing real or complex q_1 and q_2 are discussed in the following. It is recalled that the parameter B in eqn (55) is real, so that $B^2 - 4A\bar{A}$ in eqn (56) is also real. If $B^2 - 4A\bar{A}$ is non-positive, $\lambda_{1,2} = (-B \pm i\sqrt{4A\bar{A} - B^2})/2A$, and the module of the numerator is $2\sqrt{A\bar{A}}$, the same as the denominator, so that $|\lambda_{1,2}| = 1$ and q_1 and q_2 are real. For positive $B^2 - 4A\bar{A}$, $|\lambda_1/\lambda_2| = |B - \sqrt{B^2 - 4A\bar{A}}|/|B + \sqrt{B^2 - 4A\bar{A}}| \neq 1$ so that $|\lambda_1| \neq |\lambda_2|$ and q_1 and q_2 are complex conjugates. In summary, both q_1 and q_2 are real if

$$B^2 - 4A\bar{A} \leqslant 0. \tag{67a}$$

Otherwise, they are complex conjugates if

$$B^2 - 4A\bar{A} > 0. \tag{67b}$$

The displacements and stresses can be found in terms of potentials ϕ and ψ as in eqns (24) and (25). For real q_1 and q_2, the stresses have the following form in the asymptotic field:

$$\sigma_{\alpha\beta} = \frac{kA_{10}}{r^{q_1}} \tilde{\sigma}_{\alpha\beta}(\theta) \tag{68}$$

for $q_1 > q_2$ and $q_1 > 0$, where (r, θ) are the polar coordinates; k is a real constant depending on the bimaterial properties; and $\tilde{\sigma}_{\alpha\beta}$ are non-dimensional functions of the polar angle and satisfy $\tilde{\sigma}_{22}(0) = 1$. For complex conjugate q_1 and q_2, the stresses have the form

$$\sigma_{\alpha\beta} = \mathrm{Re}\left\{\frac{k'A'_{10}}{r^{q_1}}\right\} \tilde{\sigma}^{\mathrm{Re}}_{\alpha\beta}(\theta) + \mathrm{Im}\left\{\frac{k'A'_{10}}{r^{q_1}}\right\} \tilde{\sigma}^{\mathrm{Im}}_{\alpha\beta}(\theta) \tag{69}$$

where k' is a complex constant depending on the bimaterial properties and $\tilde{\sigma}^{\mathrm{Re}}_{\alpha\beta}$ and $\tilde{\sigma}^{\mathrm{Im}}_{\alpha\beta}$ are non-dimensional functions of polar angle and satisfy $\tilde{\sigma}^{\mathrm{Re}}_{\alpha\beta}(\theta = 0) = 1$. It is observed, again,

that the remote load distributions only influence the near-tip stress field through the constant A_{10} or A'_{10}.

For the limiting case of elastic/rigid bimaterial systems, $[\mu^{(2)} = \infty]$, which has been studied by Liu *et al.* (1995), the powers q_1 and q_2 are always real and are given by

$$q_1 = \frac{1}{\pi}\tan^{-1}\frac{\alpha_\ell\hat{\alpha}_s[4-(1-\hat{\alpha}_s^2)^2]}{4\alpha_\ell^2\hat{\alpha}_s^2+(1-\hat{\alpha}_s^2)^2}, \quad q_2 = 0 \tag{70}$$

where $\alpha_\ell = \alpha_{\ell 1}$ and $\hat{\alpha}_s = \hat{\alpha}_{s1}$. It is noted that q_1 becomes zero as the crack speed approaches the shear wave speed or the longitudinal wave speed, hence there is no singularity at these two limits.

For the other limiting case of homogeneous material $[\mu^{(2)} = \mu^{(1)}, \nu^{(2)} = \nu^{(1)}, \rho^{(2)} = \rho^{(1)}]$, the powers q_1 and q_2 are also real and are given by

$$q_1 = \frac{1}{\pi}\tan^{-1}\frac{4\alpha_\ell\hat{\alpha}_s}{(1-\hat{\alpha}_s^2)^2}, \quad q_2 = q_1 - \tfrac{1}{2}. \tag{71}$$

It can be shown that q_1 corresponds to the asymmetric deformation (mode II) and q_2 corresponds to the symmetric deformation (mode I). Interestingly, one can see that the orders of singularity for modes I and II are different for transonic crack growth in homogeneous solids. Due to its close relationship with geophysics, the transonic crack growth in homogeneous solids under shear mode has been studied extensively [for example, Freund (1979) and Broberg (1989)].

Liu *et al.* (1993) and Lambros and Rosakis (1995) studied the dynamic interfacial crack growth in a PMMA/steel bimaterial system. The material properties are given in Table 1. The wave speeds for the system have $c_s^{\mathrm{PMMA}} < c_\ell^{\mathrm{PMMA}} < c_s^{\mathrm{steel}} < c_\ell^{\mathrm{steel}}$. For interfacial crack speed, v, increasing from the shear wave speed, c_s^{PMMA}, to the longitudinal speed, c_ℓ^{PMMA}, of PMMA, the power of singularity exhibits the following interesting features: powers q_1 and q_2 are real for relatively low interfacial speeds (close to c_s^{PMMA}) and for relatively high speeds (close to c_ℓ^{PMMA}). However, the powers become complex conjugates for speeds in between these two ranges. This suggests that there are three sub-intervals in the range c_s^{PMMA} to c_ℓ^{PMMA}. The middle interval gives complex powers and the others lead to real powers. This trend is shown in Fig. 4 for a plane-stress PMMA/steel system, where the solid line represents the real q_1 and the dotted and dashed lines represent the real and imaginary parts $\mathrm{Re}(q_1)$ and $\mathrm{Im}(q_1)$ for complex powers, respectively. Since the interval for complex powers and the next interval for real powers are extremely small in Fig. 4a, the curves over these two intervals are replotted in Fig. 4b. It is evident that the imaginary part of the complex powers starts and ends at zero and the real part intercepts the solid lines. The power for a plane-strain PMMA/steel system is shown in Fig. 5 where the complex powers are clearly seen.

The angular stress distribution, $\tilde{\sigma}_{\alpha\beta}(\theta)$ in eqn (68), is shown in Fig. 6 for $v = 1.5\, c_s^{\mathrm{PMMA}}$, with the regularity condition $\tilde{\sigma}_{22}(\theta = 0) = 1$. There is a stress discontinuity at the PMMA/steel interface ($\theta = 0$). All stresses are singular at the characteristic angle $\theta = 90^\circ + \tan^{-1}\hat{\alpha}_{s1}$. For each stress component, the approach to infinity is exactly opposite on two sides of the characteristic angle, i.e. one to $+\infty$ and the other to $-\infty$. Figure 6 shows, again, that there is another singularity along the entire ray $\theta = 90^\circ + \tan^{-1}\hat{\alpha}_{s1}$ for transonic crack growth, besides the singularity at the crack tip.

For the other bimaterial system in Table 1, Al/Al_2O_3, the wave speeds have $c_s^{Al} < c_\ell^{Al} < c_s^{Al_2O_3} < c_\ell^{Al_2O_3}$ under plane stress conditions. The powers are shown in Fig. 7 for crack speeds between the shear and longitudinal wave speeds of aluminum. It is observed that the interval for complex powers, as marked by the dotted and dashed lines, is much larger than that for the PMMA/steel bimaterial system. This is because the elastic mismatch in the Al/Al_2O_3 system is not as severe as in the PMMA/steel system.

The powers of singularity are shown in Fig. 8 for a plane-strain Al/Al_2O_3 system. It is noted that the plane-strain longitudinal speed of aluminum is now larger than the shear

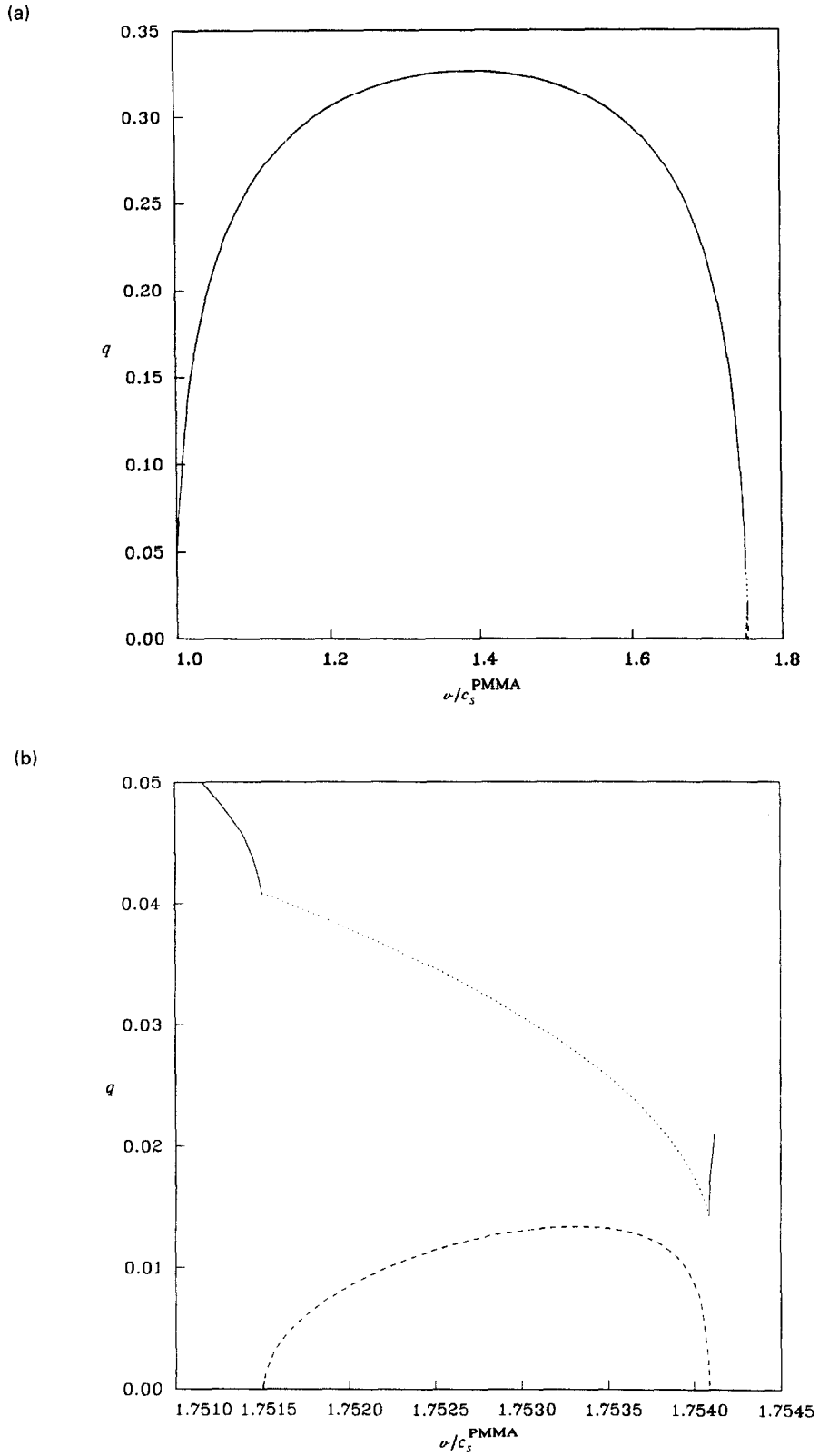

Fig. 4. Power of singularity, q, vs the normalized interfacial crack speed, v/c_s^{PMMA}, for a plane-stress PMMA/steel bimaterial system (solid line = real power q; dotted line = real part of complex q; dashed line = imaginary part of complex q). (a) Crack speed in the range $[c_s^{PMMA}, c_\ell^{PMMA}]$. (b) Crack speed close to c_ℓ^{PMMA}.

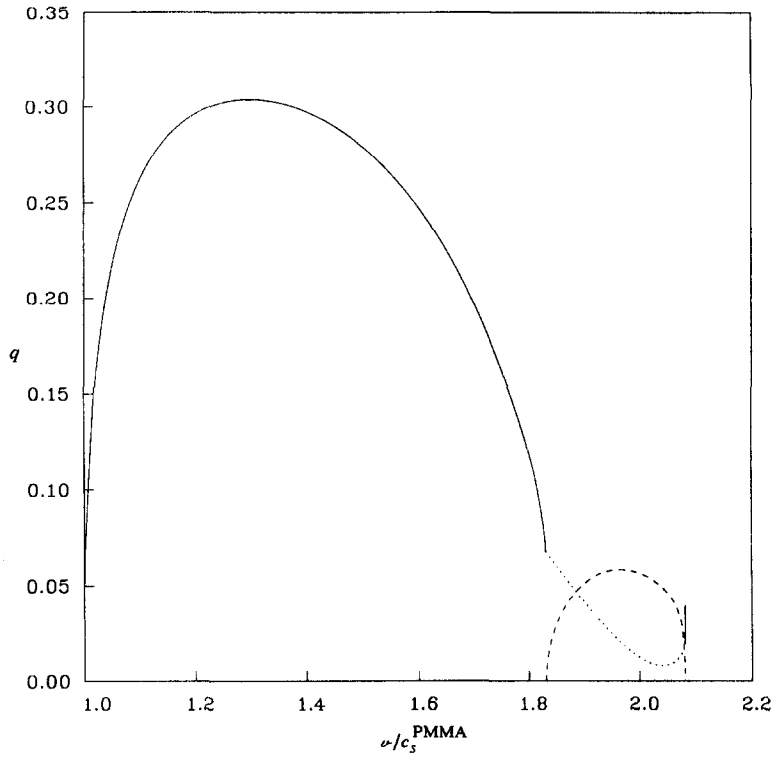

Fig. 5. Power of singularity, q, vs the normalized interfacial crack speed, v/c_s^{PMMA}, for a plane-strain PMMA/steel bimaterial system (solid line = real power q; dotted line = real part of complex q; dashed line = imaginary part of complex q); crack speed in the range $[c_s^{PMMA}, c_\ell^{PMMA}]$.

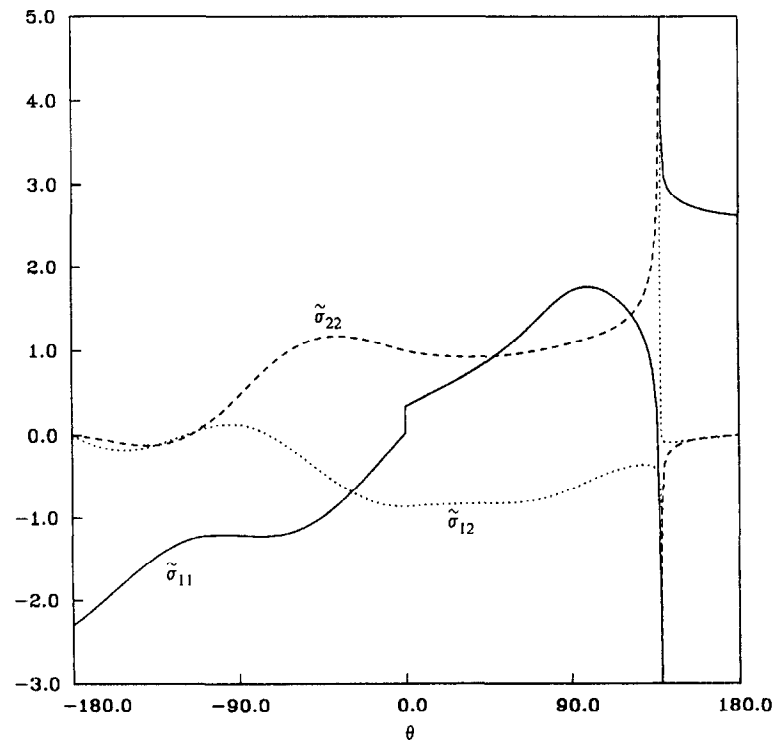

Fig. 6. The angular distribution of normalized stresses, $\tilde{\sigma}_{\alpha\beta}$ (α, β = 1, 2) for a plane-stress PMMA/steel bimaterial system with $v = 1.5c_s^{MMA}$ (solid line = $\tilde{\sigma}_{11}$; dashed line = $\tilde{\sigma}_{22}$; dotted line = $\tilde{\sigma}_{12}$).

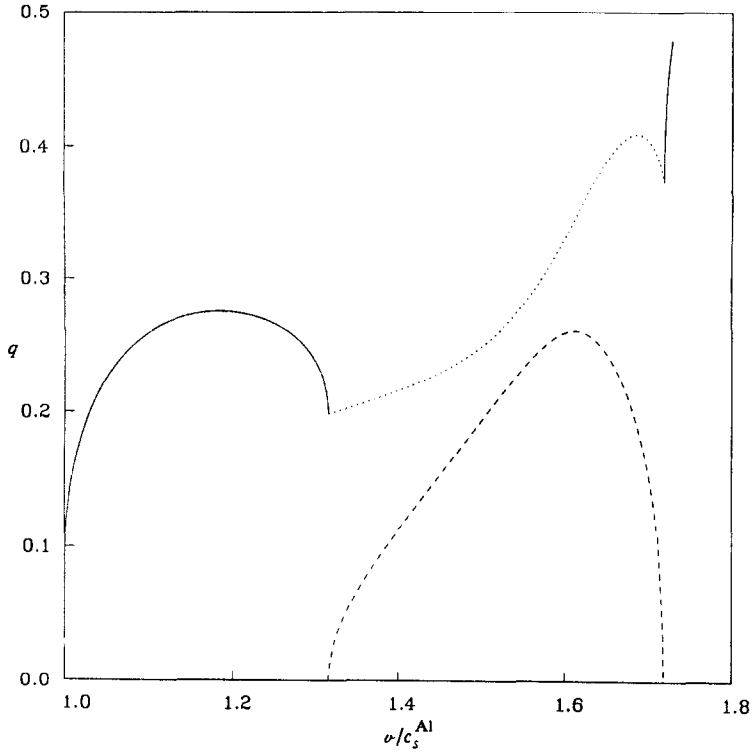

Fig. 7. Power of singularity, q, vs the normalized interfacial crack speed, v/c_s^{Al}, for a plane-stress Al/Al_2O_3 bimaterial system (solid line = real q; dotted line = real part of complex q; dashed line = imaginary part of complex q); crack speed in the range $[c_s^{Al}, c_\ell^{Al}]$.

wave speed of alumina, such that the wave speeds have $c_s^{Al} < c_s^{Al_2O_3} < c_\ell^{Al} < c_\ell^{Al_2O_3}$ (Table 1). The corresponding crack speed, v, is now limited between two shear wave speeds, c_s^{Al} and $c_s^{Al_2O_3}$. It is also observed that the Rayleigh wave speed for alumina, $c_R^{Al_2O_3} = 5519\,m\,s^{-1}$, is also within the same range.

As shown in Fig. 8a, the interval of complex powers for the plane-strain Al/Al_2O_3 system contains some features that are very different from those in Figs 4, 5, and 7. First of all, the imaginary part of the complex power, which characterizes the oscillation of the asymptotic field, approaches infinity at the Rayleigh wave speed of alumina. This means the oscillation around the transonically moving crack tip is very severe at the Rayleigh wave speed $c_R^{Al_2O_3} (> c_R^{Al})$. Moreover, the real part of the complex power has a jump of $-1/2$ across the Rayleigh wave speed, $c_R^{Al_2O_3}$. These features are better shown in Fig. 8b for crack speed v near $c_R^{Al_2O_3}$. Similar conclusions have also been established for the lower Rayleigh wave speed $c_R^{(1)}$ in the bimaterial system (Liu *et al.* 1993). For power q with a negative real part in Fig. 8a, b, the stress field near the crack tip is dominated by the T-stress, i.e. $\sigma_{12}^{(1)} = \sigma_{22}^{(1)} = \sigma_{12}^{(2)} = \sigma_{22}^{(2)} = 0$ and $\sigma_{11}^{(2)} = (E_2/E_1)\sigma_{11}^{(1)}$, where $\sigma_{11}^{(1)}$ is a constant stress that cannot be determined from the asymptotic analysis.

The angular stress distributions, $\tilde{\sigma}_{\alpha\beta}^{Re}(\theta)$ and $\tilde{\sigma}_{\alpha\beta}^{Im}(\theta)$ in eqn (69), are shown in Figs 9, respectively, for crack speed $v = 1.5\,c_s^{Al}$ corresponding to complex powers. Similar to the PMMA/steel system, the stresses for an Al/Al_2O_3 system are singular along the entire ray $\theta = 90° + \tan^{-1}\hat{\alpha}_{s1}$. Moreover, the stresses are not only oscillatory with respect to polar radius r, but are also oscillatory with respect to this characteristic angle, which can be seen from the sharp turning of the solid line in Fig. 9a. This oscillation can also be confirmed from the near-tip stress field since the stresses have terms $(\eta_1 + \hat{\alpha}_{s1}\eta_2)^{-q_1} = r^{-q_1}(\cos\theta + \hat{\alpha}_{s1}\sin\theta)^{-q_1}$, where q_1 is complex. This oscillation with polar angle is a unique feature for transonic interfacial crack growth.

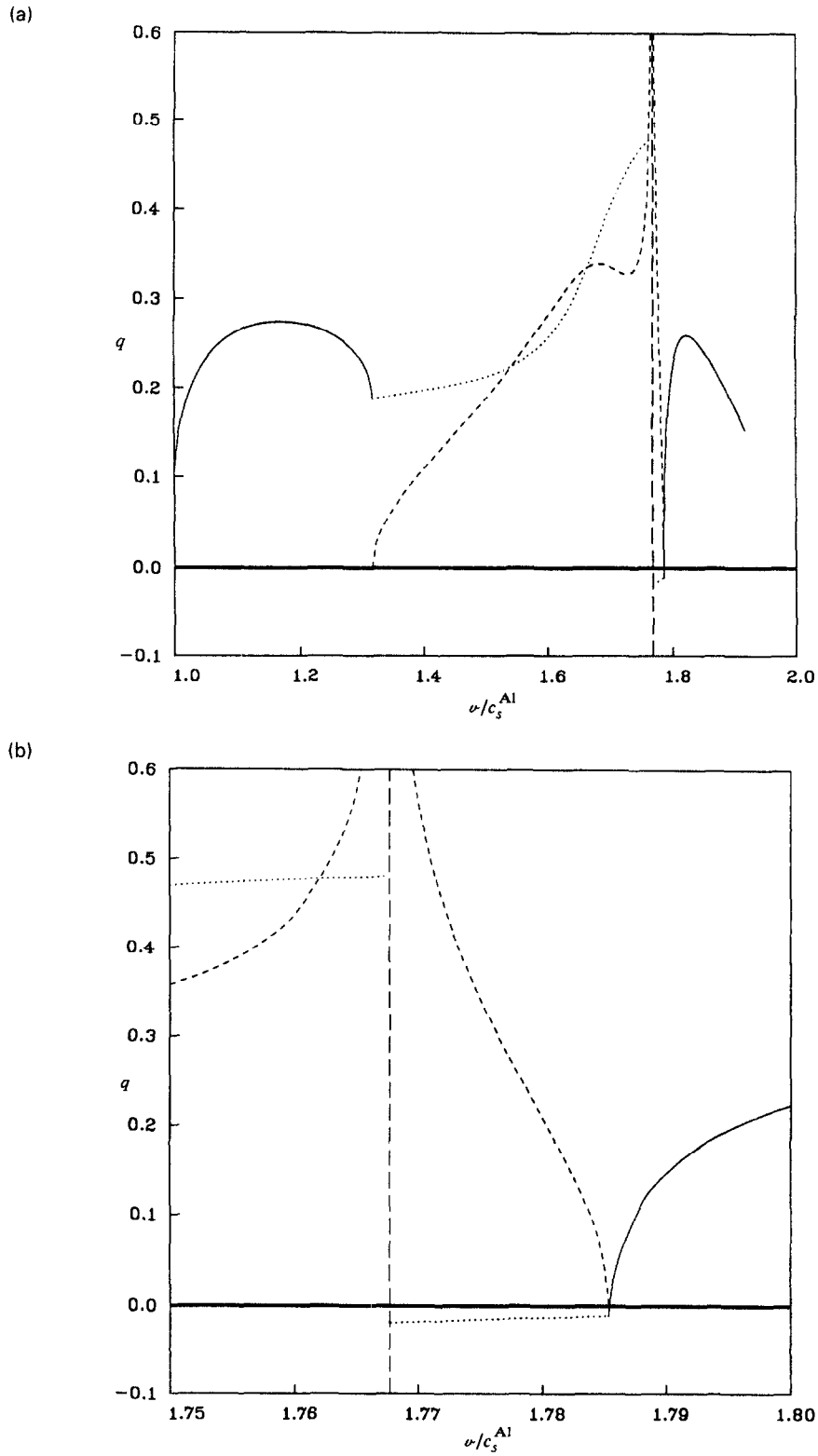

Fig. 8. Power of singularity, q, vs normalized interfacial crack speed, v/c_s^{Al}, for a plane-strain Al/Al_2O_3 bimaterial system (solid line = real q; dotted line = real part of complex q; dashed line = imaginary part of complex q). (a) Crack speed in the range $[c_s^{Al}, c_s^{Al_2O_3}]$. (b) Crack speed close to Rayleigh wave speed, $c_R^{Al_2O_3}$.

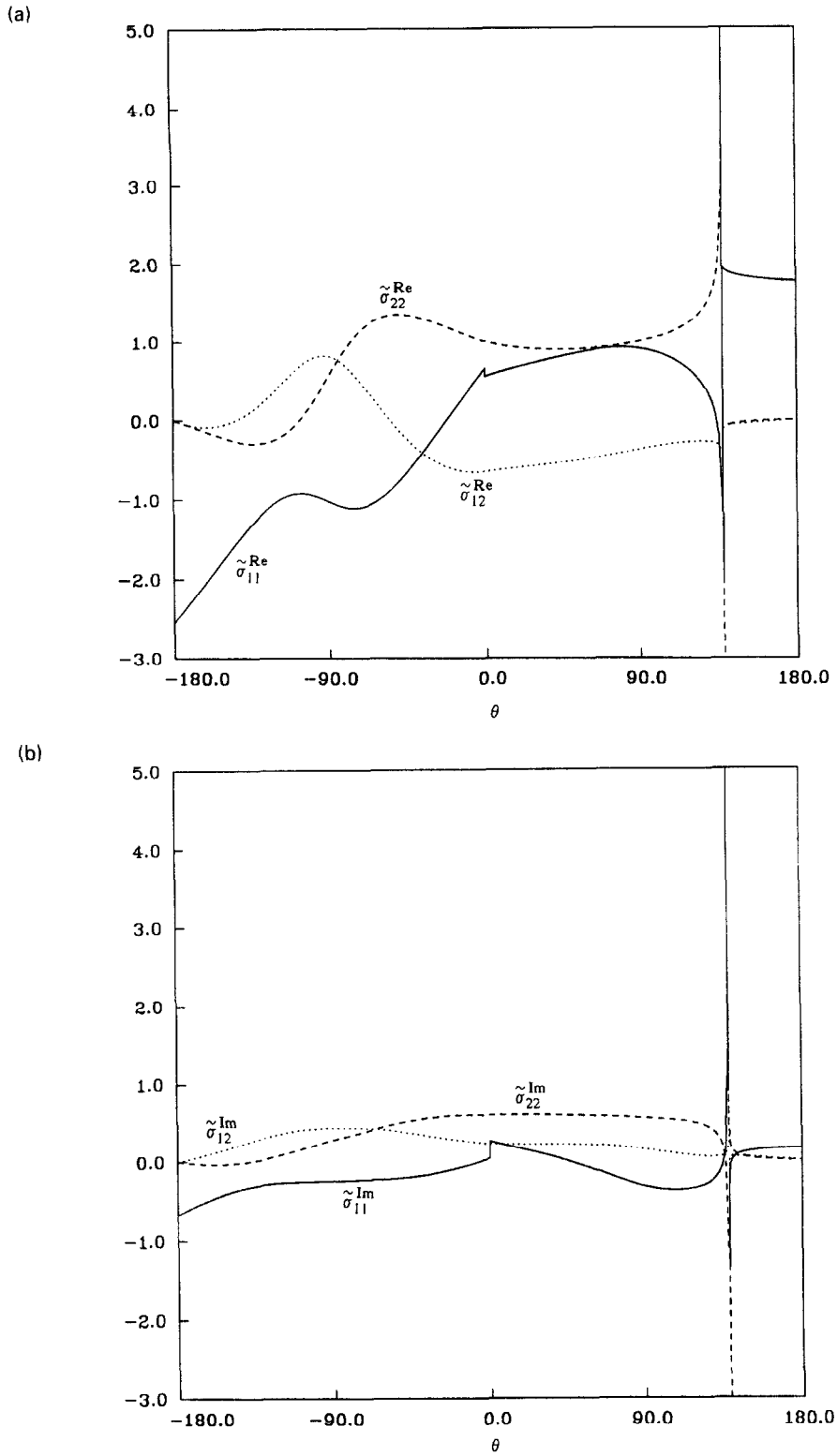

Fig. 9. The anular distribution of normalized stresses $\tilde{\sigma}_{\alpha\beta}$ ($\alpha, \beta = 1, 2$) for a plane-strain Al/Al_2O_3 bimaterial system with $v = 1.5c_s^{Al}$ (solid line = $\tilde{\sigma}_{11}$; dashed line = $\tilde{\sigma}_{22}$; dotted line = $\tilde{\sigma}_{12}$). (a) $\tilde{\sigma}^{Re}_{\alpha\beta}$. (b) $\tilde{\sigma}^{Im}_{\alpha\beta}$.

4. DISCUSSION AND CONCLUSIONS

The transonic crack growth along a bimaterial interface is studied for two systems, PMMA/steel and Al/Al_2O_3. It is found that the angular distribution of the near-tip stress field is independent of remote loading, i.e. the remote load distribution only influences the magnitude of the near-tip stress field. In the following, the superscripts 1 and 2 in the bimaterial system are chosen such that $c_s^{(1)} < c_s^{(2)}$, and the subscripts s and ℓ denote the shear wave and longitudinal wave speeds, respectively.

The following conclusions are established for the near-tip asymptotic field.

(1) The power of singularity is real and less than 1/2 for anti-plane shear deformation.

(2) For crack speeds between $c_s^{(1)}$ and $\min[c_\ell^{(1)}, c_s^{(2)}]$ (in-plane deformation), there are three sub-intervals. The powers of singularity are complex conjugates for the middle sub-interval and real for the other two. Hence, for crack speeds close to the shear wave or longitudinal wave speeds of the system, the powers of singularity are always real. Across the Rayleigh wave speed, there is a discontinuity of $-1/2$ in the real part of the complex power, and the imaginary part approaches infinity. For the limiting cases of elastic/rigid bimaterial systems and the homogeneous solid, the sub-interval for complex powers disappears.

(3) The stress field is singular, not only around the crack tip, but also on the entire ray $\eta_1 + \hat{\alpha}_{s1}\eta_2 = 0$, which has a characteristic angle $\theta = 90^\circ + \tan^{-1}\hat{\alpha}_{s1}$. Moreover, for complex powers of singularity, the stress field also oscillates around this characteristic angle.

For stationary and subsonically growing cracks, the power of the stress singularity is 1/2 (real part). However, it is observed that the power of singularity in transonic crack growth is always less than 1/2. As a result, the energy flux into the crack tip as given by Freund (1972, 1990) is always zero. This seems to be contradictory to the energy requirement for crack growth. However, similar to Broberg's (1989) study for homogeneous solids, a process zone model for the transonically moving crack tip will lead to a non-vanishing energy flux.

Acknowledgements—Y.H. gratefully acknowledges the support from the National Science Foundation (grant no. INT 94-23964) and from the ALCOA Foundation. C.L. acknowledges the Director Funded Postdoctoral Fellowship at Los Alamos National Laboratory. A.J.R. acknowledges the support from ONR (grant no. N00014-90-J-1340) and NSF (grant no. MSS-9024838).

REFERENCES

Atkinson, C. (1977). Dynamic crack problems in dissimilar media. In *Mechanics of Fracture*, Vol. 4 (Edited by G. C. Sih), pp. 213–248. Noordhoff, Leyden.

Broberg, K. B. (1989). The near-tip field at high crack velocities. *Int. J. Fract.* **39,** 1–13.

Brock, L. M. and Achenbach, J. D. (1973). Extension of an interface flaw under the influence of transient waves. *Int. J. Solids Structures* **9,** 53–67.

Deng, X. (1992). Complete complex series expansions of near-tip fields for steadily growing interface cracks in dissimilar isotropic materials. *Engng Fract. Mech.* **42,** 237–242.

Evans, A. G. and Marshall, D. B. (1989). Overview No. 85—the mechanical behavior of ceramic matrix composites. *Acta Metall.* **37,** 2567–2583.

Freund, L. B. (1972). Energy flux into the tip of an extending crack in an elastic solid. *J. Elasticity* **2,** 341–349.

Freund, L. B. (1979). The mechanics of dynamic shear crack propagation. *J. Geophys. Res.* **84,** 2199–2209.

Freund, L. B. (1990). *Dynamic Fracture Mechanics*. Cambridge University Press, Cambridge.

Gol'dstein, R. V. (1967). On surface waves in jointed elastic materials and their relation to crack propagation along the junction. *Appl. Math. Mech.* **31,** 496–502.

Lambros, J. and Rosakis, A. J. (1995) Shear dominated transonic crack growth in bimaterials—Part I: experimental observations. *J. Mech. Phys. Solids* **43,** 169–188.

Liu, C., Lambros, J. and Rosakis, A. J. (1993). Highly transient elastodynamic crack growth in a bimaterial interface: higher order asymptotic analysis and optical experiment. *J. Mech. Phys. Solids* **41,** 1887–1954.

Liu, C., Huang, Y. and Rosakis, A. J. (1995). Shear dominated transonic crack growth in bimaterials—Part II: an analytical investigation of asymptotic fields and favorable velocity regimes. *J. Mech. Phys. Solids* **43,** 189–206.

Willis, J. R. (1971). Fracture mechanics of interfacial cracks. *J. Mech. Phys. Solids* **19,** 353–368.

Willis, J. R. (1973). Self-similar problems in elastodynamics. *Phil. Trans. R. Soc. (Lond.)* **274,** 435–491.

Wu, K. C. (1991). Explicit crack-tip fields of an extending interface crack in an anisotropic bimaterial. *Int. J. Solids Structures* **27,** 455–466.

Yang, W., Suo, Z. and Shih, C. F. (1991). Mechanics of dynamic debonding. *Proc. R. Soc. Lond. A* **433,** 679–697.

Yu, H. and Yang, W. (1994). Mechanics of transonic debonding of a bimaterial interface: the anti-plane shear case. *J. Mech. Phys. Solids* **42,** 1789–1802.

APPENDIX

The eigenvalue problems in eqn (53) are solved in the following. Let

$$\chi = \bar{\mathbf{M}}\bar{\mathbf{P}}^{-1}\zeta \tag{A1}$$

where ζ is a new vector. Equation (53) can be transformed to a new eigenvalue problem

$$\bar{\mathbf{H}}\zeta = \lambda\mathbf{H}\zeta \tag{A2}$$

where $\mathbf{H} = \mathbf{M}\mathbf{P}^{-1}$ and its components, H_{ij}, are given by

$$H_{11} = \frac{\gamma[2\hat{\alpha}_{s1}\alpha_{\ell 1} - i(1-\hat{\alpha}_{s1}^2)]}{\delta} \tag{A3a}$$

$$H_{21} = \frac{\gamma\alpha_{\ell 1}(1+\hat{\alpha}_{s1}^2)}{\delta} \tag{A3b}$$

$$H_{31} = \frac{\hat{\alpha}_{s1}\alpha_{\ell 1} - i}{\delta} \tag{A3c}$$

$$H_{12} = -1 - \frac{2i\gamma\hat{\alpha}_{s1}\alpha_{\ell 2}(1-\alpha_{s2}^2)}{\eta} \tag{A3d}$$

$$H_{22} = \frac{i\gamma\alpha_{\ell 2}(1-\hat{\alpha}_{s1}^2)(1-\alpha_{s2}^2)}{\eta} \tag{A3e}$$

$$H_{32} = -\frac{[\omega + i\hat{\alpha}_{s1}\alpha_{\ell 2}(1-\alpha_{s2}^2)]}{\eta} \tag{A3f}$$

$$H_{13} = \frac{2\gamma\omega\hat{\alpha}_{s1}}{\eta} \tag{A3g}$$

$$H_{23} = 1 - \frac{\gamma\omega(1-\hat{\alpha}_{s1}^2)}{\eta} \tag{A3h}$$

$$H_{33} = \frac{[\omega\hat{\alpha}_{s1} - i\alpha_{s2}(1-\alpha_{s2}^2)]}{\eta} \tag{A3i}$$

where

$$\gamma = \frac{\mu^{(1)}}{\mu^{(2)}}, \quad \delta = 4\hat{\alpha}_{s1}\alpha_{\ell 1} - i(1-\hat{\alpha}_{s1}^2)^2, \quad \eta = (1+\alpha_{s2}^2)^2 - 4\alpha_{s2}\alpha_{\ell 2}, \quad \omega = 1+\alpha_{s2}^2 - 2\alpha_{s2}\alpha_{\ell 2}. \tag{A4}$$

The equation for λ is then, from eqn (A2),

$$\det\{\lambda\mathbf{H} - \bar{\mathbf{H}}\} = 0 \tag{A5}$$

which is equivalent to the eigenequation (54). It gives the following third-order algebraic equation:

$$(\lambda - 1)(A\lambda^2 + B\lambda + \bar{A}) = 0 \tag{A6}$$

where

$$A = \bar{\delta}Z_0 \tag{A7a}$$

$$B = \delta Z_1 + \bar{\delta}\bar{Z}_1 + 4\frac{\gamma^2}{\eta^2}\delta\bar{\delta}\alpha_{s2}\alpha_{\ell 2}(1-\alpha_{s2}^2)^2 \tag{A7b}$$

$$Z_0 = -\hat{\alpha}_{s1}\alpha_{\ell 1} + i + \frac{\gamma}{\eta}\{2\omega[2\hat{\alpha}_{s1}\alpha_{\ell 1} - i(1-\hat{\alpha}_{s1}^2)] - \delta\gamma(1-\alpha_{s2}\alpha_{\ell 2}) - (1+\hat{\alpha}_{s1}^2)(1-\alpha_{s2}^2)(\hat{\alpha}_{s1}\alpha_{\ell 2} + i\alpha_{s2}\alpha_{\ell 1})\} \tag{A7c}$$

$$Z_1 = -\bar{Z}_0 - 2\frac{\gamma}{\eta}(1+\hat{\alpha}_{s1}^2)(1-\alpha_{s2}^2)[\hat{\alpha}_{s1}\alpha_{\ell 2} - i\alpha_{s2}\alpha_{\ell 1}]. \tag{A7d}$$

It is clear that A is complex and B is real. Thus, the first two eigenvalues, λ_1 and λ_2, are the roots of the quadratic equation in eqn (A6), and $\lambda_3 = 1$ is the third eigenvalue.

The corresponding eigenvectors, χ_i, for eqn (53) can be found from

$$\{\mathbf{P}\mathbf{M}^{-1} - \lambda_i\bar{\mathbf{P}}\bar{\mathbf{M}}^{-1}\}\chi_i = 0 \quad i = 1, 2, 3, \tag{A8}$$

It is recalled that χ_1 and χ_2 can be taken as real if q_1 and q_2 are real. For complex conjugate q_1 and q_2, χ_1 and χ_2 are also complex conjugates.